Applications of path-integral renormalization group method combined with density functional theory

2007 J. Phys.: Condens. Matter 19 365230

(http://iopscience.iop.org/0953-8984/19/36/365230)

IOP PUBLISHING JOURNAL OF PHYSICS: CONDENSED MATTER

J. Phys.: Condens. Matter **19** (2007) 365230 (8pp) doi:10.1088/0953-8984/19/36/365230

Applications of path-integral renormalization group method combined with density functional theory

Yoshiki Imai[1], **Yuichi Otsuka**[2] **and Masatoshi Imada**[3]

[1] Department of Physics, Saitama University, Saitama 338-8570, Japan
[2] Synchrotron Radiation Research Center, Japan Atomic Energy Research Institute, Hyogo 679-5148, Japan
[3] Department of Applied Physics, University of Tokyo, Hongo, Bunkyo-ku, Tokyo 113-8656, Japan

E-mail: imai@phy.saitama-u.ac.jp

Received 3 December 2006, in final form 10 January 2007
Published 24 August 2007
Online at stacks.iop.org/JPhysCM/19/365230

Abstract

The path-integral renormalization group method is an efficient tool for computing electronic structure of strongly correlated electron systems. Combined with the conventional density functional approaches as a hybrid scheme, it offers a first-principles method for complex materials with involved electron correlation effects. We assess the efficiency and applicability of the hybrid scheme by examining applications to Sr_2VO_4 and YVO_3.

1. Introduction

Clarifying electronic structure of strongly correlated electron systems is one of the most challenging issues in condensed matter physics. In particular, the importance of developing first-principles numerical methods is widely recognized in the community. The density functional theory (DFT) supplemented with the local density approximation (LDA) [1, 2] offers one powerful first-principles method in general, whereas its limitation in the strongly correlated electron materials is equally well known, where strong quantum fluctuations make LDA insufficient. The insufficiency of the LDA becomes conspicuous near the Fermi level, where fluctuations and competing orders have to be seriously considered by more accurate treatments of many-body effects.

We have recently proposed a hybrid method [3] by a combination of the path-integral renormalization group (PIRG) method [4, 5] with the conventional DFT approach to overcome the difficulty of DFT in the strong correlation regime of electrons. Strong quantum fluctuations defying the DFT approach in the energy scale close to the Fermi level are treated by essentially an exact scheme of PIRG. Since the PIRG scheme costs much more computation time, we use it only for the low-energy scale near the Fermi level. This hybrid scheme allows practical, efficient and accurate computation of complicated real materials with involved spin, orbital and charge degrees of freedom. In the hybrid DFT-PIRG, we first compute the electronic structure

far from the Fermi level by using DFT with the low-energy degrees of freedom left open. This is justified when the bands near the Fermi level are rather separated from the other part as is seen in transition metal compounds and organic conductors. It enables the downfolding procedure, where the low-energy effective models are derived from the global band structure by DFT. PIRG is applied to the derived effective models to clarify properties at the low-energy scale by treating equally the spatial and dynamical fluctuations in a controllable way.

In this paper, we present recent developments achieved by DFT-PIRG applications to transition metal oxides such as Sr_2VO_4 and YVO_3, which reveal intriguing properties.

2. Method and models

2.1. Downfolding and the effective Hamiltonian

We start with the downfolding procedure by using the LDA band structure obtained from the LMTO basis functions [6]. In order to restrict the degrees of freedom to the isolated LDA bands closest to the Fermi level, we need to reduce the Hilbert space. When the states having the maximal weight near the Fermi level are denoted as $\{|d\rangle\}$ and the rest of the basis functions as $\{|r\rangle\}$, the whole Hilbert space is spanned as $\{|\chi\rangle\} = \{|d\rangle\} \oplus \{|r\rangle\}$. By eliminating the subspace $|r\rangle$, the effective tight-binding Hamiltonian for only the d-subspace is obtained.

We now derive the effective Coulomb interaction $\hat{W}_r$ at the isolated Wannier orbitals near the Fermi level after considering the screening by other bands. For efficient computation, we take two steps in deriving the screening [7]. In the first step, we employ the constrained LDA (C-LDA) method [8], where the screening from the valence bands yields W_{r1}. Hereafter, we take 3d bands as the bands near the Fermi level. When we further reduce the degrees of freedom closest to the Fermi level as for the 3d-t_{2g} bands in the recent applications to Sr_2VO_4 and YVO_3, we introduce the second step by the GW scheme [9] by taking $\hat{W}_{r1}$ as if it is the starting bare Coulomb interaction. The random-phase-approximation screening produces $\hat{W}_r(\omega) = \hat{W}_{r1}/(1 - \hat{P}_{dr}(\omega)\hat{W}_{r1})$. Here, the polarization $\hat{P}_{dr}$ represents the 3d atomic-orbital contribution contained in the e_g LDA band as well as in the oxygen 2p LDA band. Since the frequency dependence is small within the range of the t_{2g} bandwidth for transition metal oxides, the low-frequency limit $\hat{W}_r(\omega = 0)$ is taken as the interaction part $\hat{U}$ in the effective Hamiltonian [9].

The kinetic-energy part is also renormalized by the self-energy $\Sigma(k, \omega)$. This is evaluated in the GW approximation [9]. We also take into account the self-energy arising from the dynamical part of the Coulomb interaction $\hat{W}_r(\omega) - \hat{W}_r(\omega = 0)$ through the GW scheme [9]. Such a self-energy effect appears through Re Σ, and contributes to the renormalization factor $Z = (1 - \partial\Sigma/\partial\omega)^{-1}_{\omega=0}$.

Then the effective Hamiltonian is reduced to a multi-band Hubbard model:

$$\mathcal{H} = \sum_{\substack{\langle i,j\rangle \\ m,m',\sigma}} t_{ij}^{mm'} c^{\dagger}_{im\sigma} c_{jm'\sigma} + \tfrac{1}{2} \sum_{\substack{i,\alpha,\beta \\ \gamma,\delta}} U_{\alpha\beta\gamma\delta} c^{\dagger}_{i\alpha} c^{\dagger}_{i\beta} c_{i\gamma} c_{i\delta}, \tag{1}$$

in the *Wannier representation* for the t_{2g} orbital $m = (xy, yz, zx)$, where $c^{\dagger}_{im\sigma}(c_{im\sigma})$ creates (annihilates) an electron with the spin $\sigma = (\uparrow, \downarrow)$ at the site i, and $n_{im\sigma} = c^{\dagger}_{im\sigma} c_{im\sigma}$. The Greek symbols stand for the combination (m, σ) of the indices.

2.2. Path-integral renormalization group method

In order to solve the low-energy effective Hamiltonian, we employ the PIRG method [4, 5]. According to the path integral, the ground-state wavefunction is given by the projection of

the time evolution operator to the initial state. In PIRG, the ground-state wavefunction is approximately represented as a linear combination of proper basis states, $|\Psi_g\rangle = \sum_{i=1}^{L} \omega_i |\phi_i\rangle$. The operation of $\exp(-\Delta\tau H)$ and the truncation by selecting the optimized basis are iterated until the obtained lowest energy converges within the fixed Hilbert space L. Linear extrapolation to the full Hilbert space as a function of the energy variance, obtained by a systematic increase of L at large L, leads to an accurate estimate of the ground state. Recently, the quantum-number projection method was implemented in PIRG, which improves the accuracy by taking account of the symmetry of the Hamiltonian [10].

3. Application to Sr_2VO_4

3.1. Experimental properties and conventional theories of Sr_2VO_4

The transition metal compound Sr_2VO_4 has a K_2NiF_4-type (layered perovskite) structure with a strong two-dimensional anisotropy, which is analogous to the mother compound of the high-T_c superconducting material La_2CuO_4. While the electronic configuration of V^{4+} in Sr_2VO_4 is d^1 (one 3d electron), that of Cu^{2+} in La_2CuO_4 is d^9 (one 3d hole), which indicates the similarity (or duality) between the two compounds. However, the crystal-field splitting of t_{2g} orbital of V^{4+} still keeps the degeneracy of the yz and zx orbitals at lower energies than the xy orbital, which is conspicuously different from the configuration of one $3d_{x^2-y^2}$ hole in La_2CuO_4 without the orbital degeneracy. Effects of orbital fluctuations and orderings are characteristic aspects in Sr_2VO_4.

Stimulated by the duality with La_2CuO_4, several experimental studies have been carried out. The magnetic susceptibilities suggest that the ground state is an antiferromagnetic (AFM) insulator [11, 12]. The activation energy estimated from the resistivity indicates that a small Mott gap exists in Sr_2VO_4 [12, 13]. As far as we know, the spin and orbital structures are unclear. Recently, a characteristic shoulder structure has been observed in the optical conductivity for the thin film [14].

However, the conventional theoretical studies are inconsistent with the experimental results, where the LDA calculation predicts a paramagnetic metal and the unrestricted Hartree–Fock approximation (HFA) suggests a ferromagnetic (FM) insulator. In this section, considering carefully the strong correlation effects using the PIRG method combined with DFT, we investigate the ground-state properties of Sr_2VO_4 in detail [15].

3.2. Parameters determined from downfolding

After the downfolding procedure, the nearest-neighbour hopping amplitudes are -0.22 eV (xy–xy), -0.05 eV (yz–yz), and -0.19 eV (zx–zx) in the x direction. We also consider all the matrix elements up to the third-nearest-neighbour sites in the present study. On the other hand, the Coulomb interactions of the low-energy effective Hamiltonian are estimated as follows: the intraorbital terms U are 2.77 eV (xy–xy) and 2.58 eV (yz–yz, zx–zx), the interorbital terms U' are 1.35 eV (xy–yz, zx–xy) and 1.28 eV (yz–zx) and the on-site exchange terms J are 0.65 eV (xy–yz, zx–xy) and 0.64 eV (yz–zx), respectively.

3.3. Spin, orbital and charge in the ground state of Sr_2VO_4

In order to systematically study correlation effects, a parameter λ is introduced, which scales the amplitude of all the matrix elements of Coulomb interactions. The amplitude for the real material is given by $\lambda = 1$. The lattice size treated by PIRG is up to $8 \times 4 \times 1$ and $4 \times 4 \times 2$ unit cells with the periodic boundary conditions.

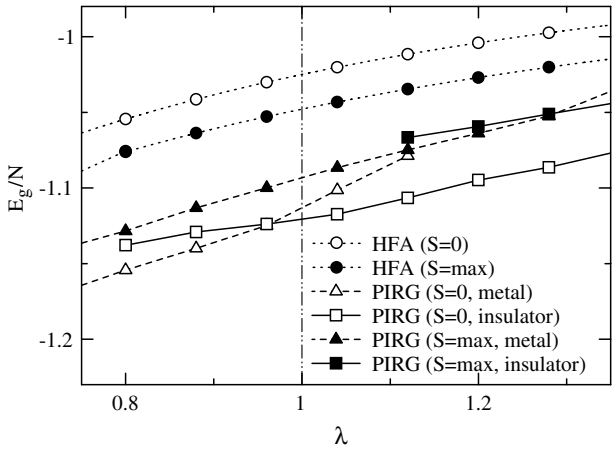

Figure 1. Ground-state energies as a function of λ obtained by HFA and PIRG calculations for $4 \times 4 \times 1$ lattice.

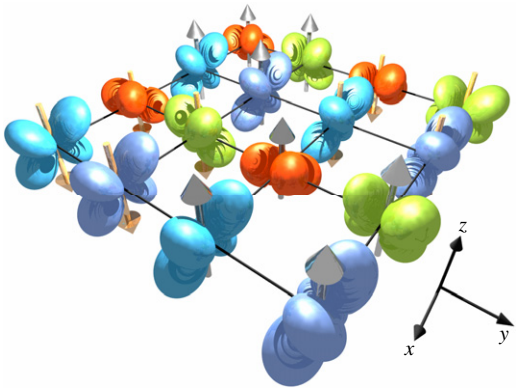

Figure 2. Ground-state spin–orbital structure of Sr_2VO_4 for $\lambda \sim 1$ and $L = 160$.

(This figure is in colour only in the electronic version)

We first present the ground-state properties of the effective Hamiltonian within the HFA as a starting point. For the two-dimensional system taken by considering the strong 2D character of Sr_2VO_4, we find that the AFM ($S = 0$) and FM ($S = \max$) states are competing. The ground state is a complete FM insulator, where the charge gap is about 0.2 eV and 2×2 orbital structure is found.

Now we show results of the PIRG calculations. Note that the dimension of the Hilbert space in PIRG is up to $L = 192$. Figure 1 shows the ground-state energy per site of the HFA and PIRG results. In comparison with the HFA energies, the PIRG results show a substantial lowering of the energy because of quantum fluctuations correctly taken into account by the projection process. Energy gains are about 0.1 eV ($S = 0$) and about 0.05 eV ($S = \max$) at $\lambda \sim 1$. In particular, for the $S = 0$ state, quantum fluctuations are very large, which indicates that the required dimension of the Hilbert space in the $S = 0$ sector is larger than that in the $S = \max$ sector in order to obtain the accurate ground-state energy. Therefore, the energy gain in the $S = 0$ sector becomes larger than that in the $S = \max$ sector. In general, the single Slater-determinant methods, such as the HFA and LDA + U method, have difficulties in describing the AFM state accurately. For this reason, the ground state obtained by PIRG becomes opposite to the HFA result. The PIRG ground state is at $S = 0$ (AFM) and insulating.

The spin and orbital patterns by PIRG show 4×2 and 2×2 super-structures, respectively, as shown in figure 2. The dominant orbitals are mostly different from those of the nearest-

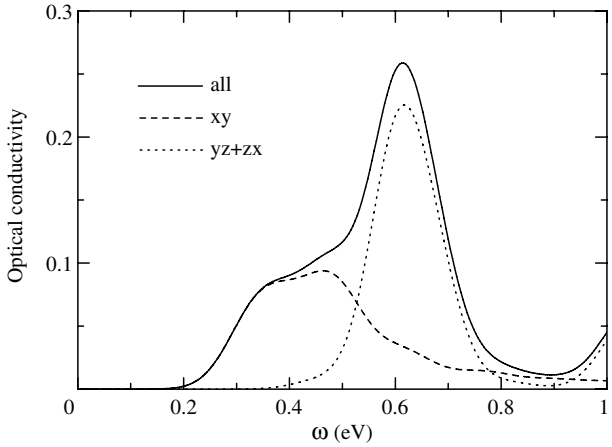

Figure 3. Optical conductivity calculated by HFA at $\lambda = 1$, $\lambda_{xy} = 0.59$, $\lambda_{yz} = 0.90$, and $\lambda_{zx} = 0.62$, which quantitatively reproduce PIRG spin–orbital structure. Solid, dashed and dotted lines stand for the total conductivity, the contribution of the xy orbital and the contribution of the yz and zx orbitals, respectively.

neighbour sites, so the FM exchange interaction between the nearest-neighbour sites is induced from the Kanamori–Goodenough rule. However, a substantial AFM interaction between the third-nearest-neighbour sites arises from the hoppings between the same orbitals. Such a magnetic frustration effect is partly the origin of a complex spin–orbital structure.

Let us discuss the metal–insulator transition in the ground state at spin sector $S = 0$. The metallic state intersects the insulating state at $\lambda \sim 0.95$. Thus the real ground state at $\lambda = 1$ belongs to the insulating ordered phase, but is close to the metal–insulator transition. This is consistent with the experimental results, which suggest that Sr_2VO_4 is the AFM Mott insulator with a small gap. For the larger system size, the obtained result is similar to that of a $4 \times 4 \times 1$ lattice. Therefore, we conclude that the system size dependence is weak.

We conclude that Sr_2VO_4 is the AFM Mott insulator with a small gap, where the complicated spin–orbital order is found (shown in figure 2). However, the energy difference between the ground state and another candidate for the $S = 0$ sector is of the order of 0.01 eV. Although we cannot exclude the possibility of the other ordered patterns, the spin–orbital structures in all candidates have long periodicities due to the existence of magnetic frustrations.

3.4. Optical conductivity

Recently, the optical conductivity has been measured on thin films [14], and shows the characteristic shoulder structure at $\omega < 1$ eV. It is difficult to investigate the dynamical physical quantities by PIRG. By employing the HFA eigenstate with the adjustable interaction parameters λ_{xy}, λ_{yz} and λ_{zx}, to reproduce physical quantities obtained by PIRG (figure 2), we calculate the optical conductivity.

Figure 3 shows the total and partial optical conductivities in the low-energy regime. Partial conductivities represent the contributions of the xy orbital and of the yz and zx orbitals. This peak structure shown in figure 3 consists of the contribution of U'–J terms. Other contributions (U' and U terms) appear at a higher energy region. In comparison with the yz and zx components, the xy spectrum becomes broader and the bandgap is strongly reduced by quantum fluctuations. Thus the shoulder structure appears, which is also consistent with the experimental result.

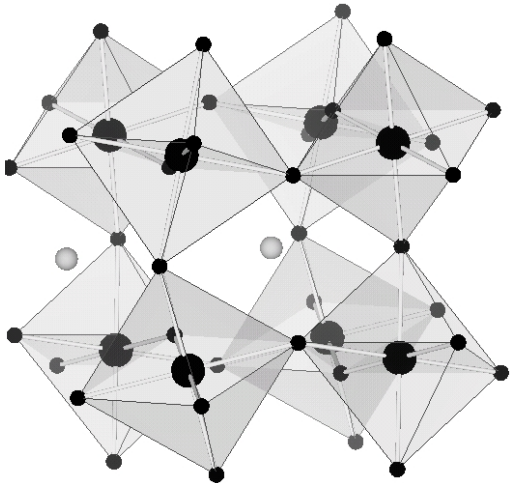

Figure 4. Crystal structure of YVO_3. Dark large and small spheres represent the V and O atoms, respectively. Light spheres are the Y atoms.

4. Application to YVO_3

4.1. Experimental properties and conventional theories of YVO_3

In this section, we discuss another application of our hybrid first-principles scheme [16]. The transition-metal oxide YVO_3 is a typical Mott insulator with a relatively large charge gap ($\sim$1 eV), where two valence electrons in the t_{2g} orbitals play a major role in the low-energy excitations. As seen in figure 4, YVO_3 has an orthorhombically distorted perovskite structure [17]. Due to the $GdFeO_3$ distortion, tilting and rotation of the VO_6 octahedra, the width of the t_{2g} bands is narrowed and mixing between these bands becomes prominent, which brings about the complicated magnetic and orbital states [17, 18]. At low temperatures, the magnetic ordering appears with AFM spin alignment both in the a–b plane and along the c axis (G-type AFM ordering). The orbital is also ordered, where all d_{xy} orbitals are singly occupied and the other electrons take the d_{yz} or d_{zx} orbital alternately in the a–b plane and the same orbital along the c axis (C-type ordering).

From the calculations based on the unrestricted HFA [19, 20], the spin ordering (SO) and the orbital ordering (OO) have been reproduced. However, as commonly seen in the HFA, they have overestimated the charge gap ($\sim$3.4 eV). Another approach to this material has been made from the first-principles calculations based on DFT with LDA. The local spin density approximation (LSDA) with the full-potential linearized augmented-plane-wave method has failed to reproduce the insulating state [21]. In addition, from the generalized gradient approximation (GGA), the ground state has resulted in the FM metal [22]. The LDA + U method has succeeded in describing the correct ground state by choosing a tuning parameter U to reproduce the experimental bandgap [22, 23].

4.2. Spin, orbital and charge in the ground state of YVO_3

Compared to Sr_2VO_4, YVO_3 is much more complicated, where two electrons on the V site ($3d^2$ configuration) are interacting with each other on the three-dimensional distorted lattice structure. Therefore, it is important to confirm whether the procedure of reducing the Hilbert space in the downfolding process works properly even in the system with largely mixed orbitals. Furthermore, YVO_3 has a much larger Mott gap than that of Sr_2VO_4. It is desired to test DFT-PIRG in totally different systems to examine a wide applicability. By considering the

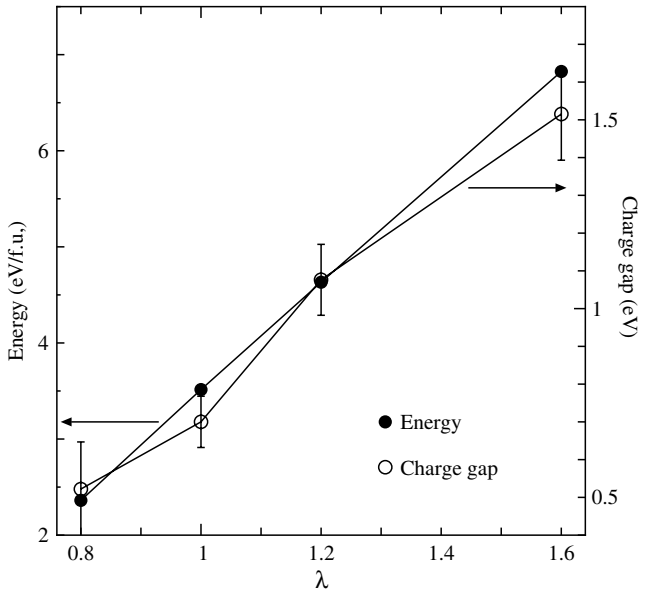

Figure 5. The λ dependence of the energy (close circles) and the charge gap (open circles).

above contrasts, YVO_3 offers a good example for this purpose. Here, we examine whether our approach is able to reproduce the magnitude of the charge gap as well as the correct ordered state from the first principles [16].

The basic procedures of the downfolding are the same as the case of Sr_2VO_4. We stress that we do not need either a procedure specific to the target materials, or tuning of the parameters. The obtained low-energy model is expressed as a three-band Hubbard-type Hamiltonian in three dimensions as in equation (1). We note that each unit cell has four V sites and each orbital has a mixture of e_g as well as t_{2g} orbitals due to the $GdFeO_3$-type lattice distortion. The values of the interactions are calculated as $U_{mm} \simeq 3.2$ eV (intraorbital Coulomb), $U_{mm'} \simeq 2.0$ eV (interorbital Coulomb) and $J_{mm'} \simeq 0.6$ eV (exchange coupling).

First we employ the HFA as a starting point of the PIRG calculations. Results of the HF solutions suggest that the ground state has the G-type SO and the C-type OO, which is consistent with the experiments. The charge gap is estimated to be $\Delta_c = 1.19$ eV, which is also comparable with the experimental result (∼1 eV). In contrast to the previous HF results [19, 20], our effective model gives a good starting point to discuss the gap amplitude as well as the order patterns.

Using the HF solutions, we proceed to the PIRG calculations. We have performed the calculations up to $L = 192$ on the system with the 32 V sites. The ground-state energy is estimated by extrapolating the energy linearly with its variance. Figure 5 shows the λ dependence of the energy and gap, where λ is again the scaling parameter for the interaction. Compared with the HF solutions, the charge gap obtained by PIRG is reduced by 30–40% due to the quantum fluctuations. For the realistic case ($\lambda = 1$), the charge gap is 0.70 ± 0.07 eV, which is rather smaller than the experimental estimate of the gap. We note that the experimental gap is obtained from the optical conductivity, that is, the direct gap. On the other hand, PIRG calculation gives the indirect gap, which in general should be smaller than the direct gap. Although the indirect gap is not known so far in experiments, the gap amplitudes seem to be consistent with each other. It has prominently improved the estimation in comparison with the HF or DFT results.

5. Concluding remark

By applying DFT-PIRG methods, some of the transition metal oxides are treated to assess the efficiency of the method for strongly correlated systems. Physical properties of Sr_2VO_4 show the AFM insulator with a small gap, consistent with the experimental results. The optical conductivity shows a shoulder structure, which all reproduces the experimental result. The ground-state spin–orbital structure is predicted to have a complex pattern with long periodicity. For the cubic perovskite oxide YVO_3, the PIRG result of spin and orbital ordering at the ground state is consistent with the experiments. In addition, the gap amplitude, which is comparable with the experiments, is obtained from the first principles without any adjustable parameters. The two test cases have proven that DFT-PIRG is a promising tool for difficult problems of correlated electrons. More controversial and challenging problems such as properties of cuprate and organic superconductors are planned as the subjects in the future applications.

Acknowledgments

The authors would like to thank Igor Solovyev for valuable support. This work is partially supported by a grant-in-aid for scientific research from the Ministry of Education, Culture, Sports, Science and Technology under grant No 17064004.

References

[1] Hohenberg P and Kohn W 1964 *Phys. Rev.* B **138** 864
[2] Kohn W and Sham L J 1965 *Phys. Rev.* A **140** 1133
[3] Imai Y, Solovyev I and Imada M 2005 *Phys. Rev. Lett.* **95** 176405
[4] Imada M and Kashima T 2000 *J. Phys. Soc. Japan* **69** 2723
[5] Kashima T and Imada M 2001 *J. Phys. Soc. Japan* **70** 2287
[6] Andersen O K 1975 *Phys. Rev.* B **12** 3060
Gunnarsson O, Andersen O K and Jepsen O 1984 *Phys. Rev. Lett.* **53** 2571
[7] Solovyev I V and Imada M 2005 *Phys. Rev.* B **71** 045103
[8] Dederichs P H *et al* 1984 *Phys. Rev. Lett.* **53** 2512
[9] Aryasetiawan F, Imada M, Georges A, Kotliar G, Biermann S and Lichtenstein A I 2004 *Phys. Rev.* B **70** 195104
[10] Mizusaki T and Imada M 2004 *Phys. Rev.* B **69** 125110
[11] Cyrot M, Lambert-Andron B, Soubeyroux J L, Rey M J, Dehauht Ph, Cyrot-Lackmann F, Fourcaudot G, Beille J and J L 1990 *J. Solid State Chem.* **85** 321
[12] Nozaki A, Yoshikawa H, Wada T, Yamauchi H and Tanaka S 1991 *Phys. Rev.* B **43** 181
[13] Matsuno J, Okimoto Y, Kawasaki M and Tokura Y 2003 *Appl. Phys. Lett.* **82** 194
[14] Matsuno J, Okimoto Y, Kawasaki M and Tokura Y 2005 *Phys. Rev. Lett.* **95** 176404
[15] Imai Y and Imada M 2006 *J. Phys. Soc. Japan* **75** 094713
[16] Otsuka Y and Imada M 2006 *J. Phys. Soc. Japan* **75** 124707
[17] Kawano H, Yoshizawa H and Ueda Y 1994 *J. Phys. Soc. Japan* **63** 2857
[18] Miyasaka S, Okimoto Y and Tokura Y 2003 *Phys. Rev.* B **68** 100406
[19] Mizokawa T and Fujimori A 1996 *Phys. Rev.* B **54** 5368
[20] Mizokawa T, Khomskii D I and Sawatzky G A 1999 *Phys. Rev.* B **60** 7309
[21] Sawada H, Hamada N, Terakura K and Asada T 1996 *Phys. Rev.* B **53** 12742
[22] Sawada H and Terakura K 1998 *Phys. Rev.* B **58** 6831
[23] Fang Z, Nagaosa N and Terakura K 2003 *Phys. Rev.* B **67** 035101